Molecular Crystals and Liquid Crystals
Publication details, including instructions for authors and subscription information:
http://www.tandfonline.com/loi/gmcl16

Solitons Generated by Pressure Gradients in Nematic Liquid Crystals

Shu Changqing [a] & Lin Lei [b c d]

[a] Institute of Physics, Chinese Academy of Sciences, Beijing, China

[b] Department of Physics, City College, City University of New York, New York, N.Y., 10031, USA

[c] Department of Physics, Queensborough Community College, City University New York, Bayside, N.Y., 11364, USA

[d] Institute of Physics, Chinese Academy of Sciences, Beijing, China

Version of record first published: 20 Apr 2011.

To cite this article: Shu Changqing & Lin Lei (1985): Solitons Generated by Pressure Gradients in Nematic Liquid Crystals, Molecular Crystals and Liquid Crystals, 131:1-2, 47-68

To link to this article: http://dx.doi.org/10.1080/00268948508084192

Mol. Cryst. Liq. Cryst., 1985, Vol. 131, pp. 47–68
0026-8941/85/1312–0047/$25.00/0

Solitons Generated by Pressure Gradients in Nematic Liquid Crystals†

SHU CHANGQING

Institute of Physics, Chinese Academy of Sciences, Beijing, China

and

LIN LEI

Department of Physics, City College, City University of New York, New York, N.Y. 10031, USA,‡ and Department of Physics, Queensborough Community College, City University New York, Bayside, N.Y. 11364, USA, and Institute of Physics, Chinese Academy of Sciences, Beijing, China

(*Received January 22, 1985*)

Equations of motion of director and velocity of nematic liquid crystals under pressure gradients are derived from the Ericksen-Leslie theory. Under suitable approximations, these coupled equations are reduced to a single (2 + 1) nonlinear partial differential equation for the director angle. Boundary effects are taken into account. Similarity analysis of this equation is presented. Properties of steady-state solutions are discussed. Numerical solutions are obtained. Traveling solutions of the (2 + 1) equation are given numerically showing the existence of solitons propagating along the direction of the pressure gradient (in both directions). Corresponding optical interference patterns of these solitons under both monochromatic and white lights are calculated. Good agreement between our theoretical results and recent experiments are obtained.

I. INTRODUCTION

Solitons in liquid crystals is a fascinating subject of much recent interest.[1–3] In particular, the existence of propagating solitons in uni-

†Paper presented at the Tenth International Liquid Crystal Conference, York, United Kingdom, July 16-20, 1984.

‡Correspondence address.

form, steady-shearing nematics was first pointed out by Lin et al.[3,4] Relevant experiments[5] were analysed and interpreted[3,4] as experimental evidence of these solitons. Also, effects of external (magnetic or electric) fields on these solitons are given.[6] Analytic forms of these solitons (at high speed), together with their energies and classifications, are provided in References 2, 3 and 6. More recently, multi-solitons, time evolution and decomposition of initial state,[2] two-dimensional anaylsis[7] and proper determination of the distribution of director angles[8] (as function of space and time coordinates) from experimental data are investigated. Furthermore, time-dependent unsteady shearing nematics have been studied[9] by the multiple scales perturbation method[10] and solitons are found to travel with time-dependent velocities.

The natural questions to be asked are: Can solitons also exist in nematics under other circumstances? If so, how do they differ from those[3,6] above?

The present paper is a theoretical investigation of nematics under one-dimensional pressure gradients. Solitons are indeed found to exist in this case (Section V). The governing equation (Section II) is no longer the damped, driven sine-Gordon equation used in the uniform shearing case.[3,6] Our theoretical results are in good agreement with experiments[11,7] (Section VI).

II. EQUATIONS OF MOTION

Let us assume that a constant pressure gradient is applied in the x direction to a nematic. Possible transverse flows are inhibited by the boundaries of the liquid crystal cell in practice (see References 7 and 11). We therefore start with the ideal situation that

$$\begin{aligned} \mathbf{v} &= (v_x, v_y, 0) \\ \mathbf{n} &= (\sin\theta, \cos\theta, 0) \end{aligned} \tag{2.1}$$

and

$$\begin{aligned} v_x &= v_x(x,y,t),\ v_y = v_y(x,y,t), \\ \theta &= \theta(x,y,t),\ p = p(x,y) \end{aligned} \tag{2.2}$$

where $\mathbf{v}$, $\mathbf{n}$ and p are the velocity, director and pressure, respectively. (In Section VI, y is taken as the normal of the liquid crystal cell surfaces.) Under Eqs.(2.1) and (2.2), the Ericksen-Leslie equations[12]

become (notations below are adopted from Reference 13)

$$M\frac{d^2\theta}{dt^2} = K\left(\frac{\partial^2\theta}{\partial x^2} + \frac{\partial^2\theta}{\partial y^2}\right) - \gamma\frac{d\theta}{1dt} + \tfrac{1}{2}\gamma_1\left(\frac{\partial v_x}{\partial y} - \frac{\partial v_y}{\partial x}\right)$$

$$-\tfrac{1}{2}\gamma_2\left(\frac{\partial v_x}{\partial x} - \frac{\partial v_y}{\partial y}\right)\sin 2\theta - \tfrac{1}{2}\gamma_2\left(\frac{\partial v_x}{\partial y} + \frac{\partial v_y}{\partial x}\right)\cos 2\theta \quad (2.3)$$

$$\rho\frac{dv_x}{dt} = \frac{\partial p}{\partial x} - K\frac{\partial}{\partial x}\left(\frac{\partial\theta}{\partial x}\right)^2 - K\frac{\partial}{\partial y}\left(\frac{\partial\theta}{\partial x}\frac{\partial\theta}{\partial y}\right) + \frac{\partial}{\partial x}\sigma'_{xx} + \frac{\partial}{\partial y}\sigma'_{xy} \quad (2.4)$$

$$\rho\frac{dv_y}{dt} = -\frac{\partial p}{\partial y} - K\frac{\partial}{\partial y}\left(\frac{\partial\theta}{\partial y}\right)^2 - K\frac{\partial}{\partial x}\left(\frac{\partial\theta}{\partial x}\frac{\partial\theta}{\partial y}\right) + \frac{\partial}{\partial x}\sigma'_{yx} + \frac{\partial}{\partial y}\sigma'_{yy} \quad (2.5)$$

where the moment of inertia density M is denoted by ρ_1 in Reference 13, ρ is the density. In Eqs. (2.3)-(2.5), for simplicity, the one-constant approximation ($K_1 = K_2 = K_3 = K$) is used, and

$$\begin{aligned}
\sigma'_{xx} &= (\alpha_2 + \alpha_3)(d\theta/dt - \omega_{xy})\cos\theta\sin\theta + [(\alpha_5 + \alpha_6)\sin\theta\cos\theta \\
&\quad + 2\alpha_1\sin^3\theta\cos\theta]d_{xy} + (-\alpha_1\sin^2\theta\cos\theta + \alpha_4 + \alpha_5\sin^2\theta + \alpha_6\sin^2\theta)d_{xx} \\
\sigma'_{xy} &= (\alpha_2\cos^2\theta - \alpha_3\sin^2\theta)(d\theta/dt - \omega_{xy}) + (\alpha_4 + \alpha_5\cos^2\theta + \alpha_6\sin^2\theta \\
&\quad + 2\alpha_1\sin^2\theta\cos^2\theta)d_{xy} + (-\tfrac{1}{2}\alpha_1\sin 2\theta\cos 2\theta + \alpha_5\sin\theta\cos\theta \\
&\quad - \alpha_6\sin\theta\cos\theta)d_{xx} \qquad (2.6) \\
\sigma'_{yx} &= (\alpha_3\cos^2\theta - \alpha_2\sin^2\theta)(d\theta/dt - \omega_{xy}) + (2\alpha_1\sin^2\theta\cos^2\theta + \alpha_4 \\
&\quad + \alpha_5\sin^2\theta + \alpha_6\cos^2\theta)d_{xy} + [(\alpha_6 - \alpha_5)\sin\theta\cos\theta - \tfrac{1}{2}\alpha_1\sin 2\theta\cos 2\theta]d_{xx} \\
\sigma'_{yy} &= -(\alpha_2 + \alpha_3)(d\theta/dt\,\omega_{xy})\sin\theta\cos\theta + [2\alpha_1\sin\theta\cos^3\theta \\
&\quad + (\alpha_5 + \alpha_6)\sin\theta\cos\theta]d_{xy} - (\alpha_2\cos^2\theta\cos 2\theta + \alpha_4 + \alpha_5\cos^2\theta + \alpha_6\cos^2\theta)d_{xx}
\end{aligned}$$

where

$$d_{xy} = \tfrac{1}{2}(\partial v_x/\partial y + \partial v_y/\partial x),\ \omega_{xy} = \tfrac{1}{2}(\partial v_x/\partial y - \partial v_y/\partial x),\ \text{etc.} \quad (2.7)$$

In Eq. (2.6), the incompressibility condition,

$$\partial v_x/\partial x + \partial v_y/\partial y = 0 \quad (2.8)$$

has been used.

The four coupled equations (2.3)-(2.5) and (2.8) (for the four unknowns θ, v_x v_y and p) are obviously too complicated to be solved exactly. Some kind of approximation is needed.

Note that $\rho \sim 1$ gm cm^{-3}, $M \sim 10^{-12}$ gm cm^{-1}. In the experiments of References 7 and 11, the x and y dimensions of the liquid crystal cell are typically 20 cm and 50 μm, respectively (the glass surfaces are in the x-z plane), velocity of the observed wave $c \sim 10$ cm s^{-1} and $p \sim 10^4$ dyn cm^{-2}. With a characteristic time $t_0 \sim 0.1$ s one may estimate the order of magnitude of each term in Eqs.(2.3)-(2.5). Keeping only the highest-order terms and other relevant terms, Eqs.(2.3)-(2.5) are simplified to

$$K\frac{\partial^2\theta}{\partial x^2} + K\frac{\partial^2\theta}{\partial y^2} - \gamma_1\frac{\partial\theta}{\partial t} + \tfrac{1}{2}(\gamma_1 - \gamma_2\cos 2\theta)\frac{\partial v_x}{\partial y} = 0 \quad (2.9)$$

$$-\frac{\partial p}{\partial x} + \frac{\partial}{\partial y}\left[\phi_1(\theta)\frac{\partial\theta}{\partial t} + \phi_2(\theta)\,\tfrac{1}{2}\frac{\partial v_x}{\partial y}\right] = 0 \quad (2.10)$$

$$-\frac{\partial p}{\partial y} = 0 \quad (2.11)$$

where

$$\phi_1(\theta) \equiv \alpha_2\cos^2\theta - \alpha_3\sin^2\theta = \phi_1(-\theta)$$

$$\phi_2(\theta) \equiv \alpha_4 + \alpha_5\cos^2\theta + \alpha_6\sin^2\theta + 2\alpha_1\sin^2\theta\cos^2\theta - \phi_1(\theta) \quad (2.12)$$

$$= \phi_2(-\theta)$$

Equation (2.11) implies $p = p(x)$. Integrating Eq.(2.10) once with

respect to y (taking the constant of integration to be zero) and combining with Eq.(2.9) one has

$$K\frac{\partial^2\theta}{\partial x^2} + K\frac{\partial^2\theta}{\partial y^2} - \frac{\partial\theta}{\partial t}\left[\gamma_1 + (\gamma_1 - \gamma_2\cos 2\theta)\frac{\phi_1(\theta)}{\phi_2(\theta)}\right] + \left(\frac{\gamma_1 - \gamma_2\cos 2\theta}{\phi_2(\theta)}\right)\frac{\partial p}{\partial x}y = 0 \quad (2.13)$$

In dimensionless form, Eq.(2.13) becomes

$$\frac{\partial^2\theta}{\partial X^2} + \frac{\partial^2\theta}{\partial Y^2} - f(\theta)\frac{\partial\theta}{\partial T} + g(\theta)QY = 0 \quad (2.14)$$

where (assuming $\gamma_2 < 0$ for real materials[3])

$$\begin{aligned} &X \equiv x/\lambda, Y \equiv y/\lambda, T \equiv t/\tau, \gamma \equiv \gamma_1/|\gamma_2|, \gamma_1 = \alpha_3 - \alpha_2, \\ &\gamma_2 = \alpha_3 + \alpha_2, \tau \equiv |\gamma_2|/p_0, P \equiv p/p_0, \lambda \equiv (K/p_0)^{\frac{1}{2}}, Q \equiv \partial P/\partial X, \\ &f(\theta) \equiv \gamma - \tfrac{1}{2}(\gamma + \cos 2\theta)^2|\gamma_2|/\phi_2(\theta) = f(-\theta), \\ &g(\theta) \equiv (\gamma + \cos 2\theta)|\gamma_2|/\phi_2(\theta) = g(-\theta) \end{aligned} \quad (2.15)$$

and p_0 is an arbitrary but constant value of the pressure p.

For a homeotropic cell, the boundary condition is

$$\Theta(X, \pm D/2, T) = 0 \quad (2.16)$$

For planar cell,

$$\theta(X, \pm D/2, T) = \pi/2 \quad (2.17)$$

where the two glass plates are located at $y = \pm d/2$, and $D \equiv d/\lambda$.

Equation (2.14) [or (2.13)] is the basic (2 + 1) nonlinear partial differential equation to be investigated below. It is more complicated than the damped, driven sine-Gordon equation governing the uniforms shearing case [see Eq. (1) of Reference 3]. Solutions of Eq. (2.14) have the symmetries,

$$\theta(X, -Y; Q) = -\theta(X, Y; Q) = \theta(X, Y; -Q) \quad (2.18)$$

General properties of Eqs. (2.14), (2.16) and (2.17) will be given in Sections III to V.

III. SIMILARITY ANALYSIS

It is possible to relate the physical quantities in two different liquid crystal cells by a similarity analysis. Using subscripts 1 and 2 to denote the two cells it is not difficult to see that, under the conditions that the material parameters (α_1, γ_i) are identical and

$$D_1 = D_2,\ Q_1 = Q_2,\ C_1 = C_2 \tag{3.1}$$

solutions of Eqs. (2.14), (2.16) and (2.17) for the two cells (in dimensionless forms) are identical to each other. Here, C is a typical velocity, e.g., the velocity of a traveling wave in the X direction (see Section V). Denoting

$$\lambda_1/\lambda_2 \equiv \mu \tag{3.2}$$

Eq. (3.1) implies that

$$\begin{aligned} &(p_0)_1/(p_0)_2 = \mu^{-2},\ \tau_1/\tau_2 = \mu^2, \\ &(\partial p/\partial x)_1/(\partial p/\partial x)_2 = \mu^{-3},\ c_1/c_2 = \mu^{-1} \end{aligned} \tag{3.3}$$

where $c \equiv C\,\lambda/\tau$. For two cells satisfying the conditions of Eq. (3.1), their respective physical quantities are given in Table I, where μ is an arbitrary positive number. Here, n_0 and n_e are assumed to be the same for the two cells and δ is the width of dark line in the transmitted white (or monochromatic) light pattern (see Section V).

For example, for two cells of thickness $d_1 = 36$ μm and $d_2 = 22$ μm, respectively (as used in the experiments[11,7]), we have $\theta = d_1/d_2 = 1.636$. If we apply pressure gradients such that $(\partial p/\partial x)_1/(\partial p/\partial x)_2 =$

TABLE I

Physical quantities of two liquid crystal cells having similar solutions [i.e. satifying Eq. (3.1)].

Cell number	Cell thickness	Pressure gradient	Wave velocity	Dark-line width
#1	d	$\partial p/\partial x$	c	δ
#2	$\mu^{-1}d$	$\mu^{-3}(\partial p/\partial x)$	μc	$\mu^{-1}\delta$

$\mu^{-3} = 0.228$, we will find that $\delta_1/\delta_2 = \mu = 1.636$ corresponding to the two waves with $c_1/c_2 = \mu^{-1} = 0.611$ in the two cells.

IV. STEADY STATES

For the steady state ($\partial\theta/\partial T = 0$) which is uniform in X, $\theta = \theta(Y)$, Eq. (2.14) becomes

$$d^2\theta/dY^2 + g(\theta)QY = 0 \tag{4.1}$$

Noting that the boundary condition Eq. (2.16) or (2.17) is unchanged under $(\theta, Y) \to (-\theta, -Y)$, one obtains

$$\theta(Y = 0) = 0 \tag{4.2}$$

By Eq. (2.18), $\theta(-Y; Q) = -\theta(Y; Q)$; we may discuss only the region of $Y > 0$. Let

$$u \equiv \frac{2}{3} Y^{3/2} \tag{4.3}$$

Eq. (4.1) becomes

$$d^2\theta/du^2 + (3u)^{-1}d/\theta/du + g(\theta)Q = 0 \tag{4.4}$$

We now confine our discussion to the homeotropic case of Eq. (2.16). We thus have

$$\theta(u = 0) = \theta(u = u_0) = 0 \tag{4.5}$$

where $u_0 \equiv \frac{2}{3}(D/2)^{3/2}$. Integrating Eq. (4.4) once we have

$$\tfrac{1}{2}(d\theta/du)^2 + F(\theta) - F(\theta_m) + G(\theta) - G(\theta_m) = 0 \tag{4.6}$$

where

$$F(\theta) - F(\theta_m) = \int_{u(\theta m)}^{u(\theta)} \frac{du}{3u} \left(\frac{d\theta}{du}\right)^2 \tag{4.7}$$

$$G(\theta) - G(\theta_m) = \int_{\theta m}^{\theta} g(\theta) Q d\theta \tag{4.8}$$

and θ_m is a constant given by $(d\theta/du)_{\theta=\theta m} = 0$. The existence of θ_m is guaranteed by Eq. (4.5) and the mean-value theorem. By Eq. (4.6) and $(d\theta/du)^2 \geqslant 0$, we see that no solution can exist in the domain such that

$$G(\theta_m) - G(\theta) + F(\theta_m) - F(\theta) < 0 \tag{4.9}$$

It can be shown that such regions of θ indeed exist and there are multiple solutions of $\theta(Y)$ corresponding to each Q.[7] In some of these solutions, it is possible that $\theta_m > \theta_0$, the alignment angle given by $\pi/4 < \theta_p \equiv \cos^{-1}(-\gamma) < \pi/2$. These solutions may be excited experimentally when the supplied energy is high.

Figure 1 shows numerical solutions of Eqs. (4.1) and (2.16) with $D/2 = 12.5$ and $Q = 0.001, 0.005, 0.01$ and 0.03 respectively. Here, θ_m is the maximum angle and $\theta_m < \theta_0$. The parameters $\gamma = 0.96$, $\gamma_1 = 0.77P$, $\alpha_1 = 0.065P$, $\alpha_4 = 0.83P$, $\alpha_5 = 0.46P$, $\alpha_6 = -0.35P$ for

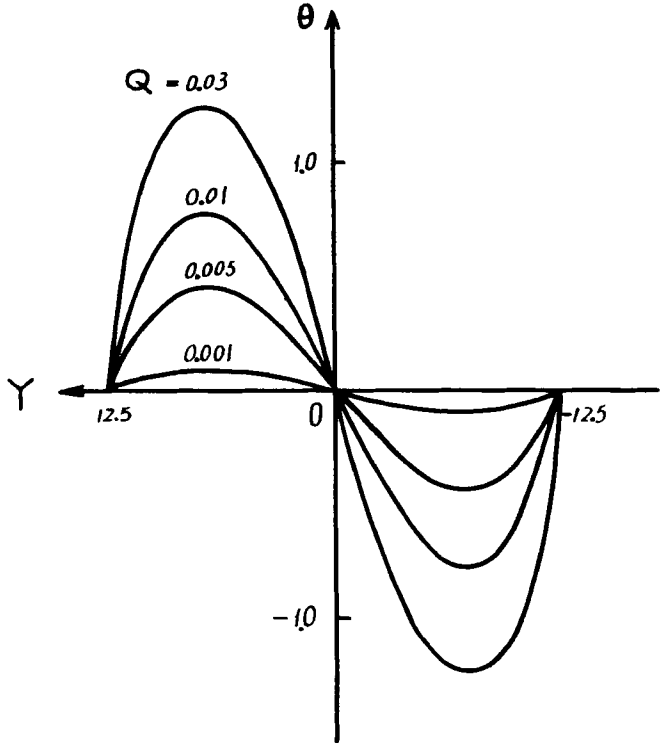

FIGURE 1 X-independent steady-state solution θ vs. Y. $Q > 0$ and $D = 25$.

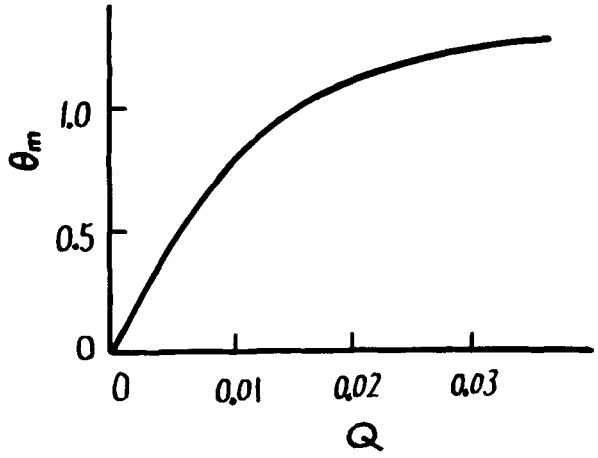

FIGURE 2 Maximum angle θ_m from Figure 1 as function of Q.

MBBA are used. θ_m from Figure 1 as function of Q is plotted in Figure 2.

V. SOLITONS

For traveling wave $\theta = \theta(Y, Z)$, $Z \equiv X - CT$, Eq. (2.14) becomes

$$\partial^2\theta/\partial Z^2 + \partial^2\theta/\partial Y^2 - Cf(\theta)\partial\theta/\partial Z + g(\theta)QY = 0 \qquad (5.1)$$

Eq. (5.1) is too complicated to be solved analytically. We thus solve Eq. (5.1) numerically under the homeotropic boundary conditon

$$\theta(Y = \pm D/2, Z) = 0 \qquad (5.2)$$

and the free boundary condition

$$(\partial\theta/\partial Z)_{Z=\pm L} = 0 \qquad (5.3)$$

where $2L$ is the width of the mesh used in the Z direction. The details are given in Appendix A. The planar case can be solved similarly.

Note that solutions of Eq. (5.1) are related by

$$\begin{aligned}\theta(Z,Y;Q,C) &= \theta(Z,-Y;-Q,C) = -\theta(Z,Y;Q,-C) \\ &= -\theta(Z,-Y;Q,C) = -\theta(Z,Y;-Q,C)\end{aligned} \qquad (5.4)$$

A. Single solitons

In Figure 3(a), solution of Eqs. (5.1)-(5.3) with $Q = 0.03$ and $C = 30$ is plotted. Material parameters for MBBA as in Figure 1 are adopted. Note that $\theta = 0$ at $Y = 0, \pm D/2$ and also at $Z = 0$. For fixed Y between 0 and $D/2$, the curve θ vs. Z looks like the A-soliton [Eq. (A8), see also Figure 3(a) of Reference 6 or Figure 3 of Reference 2]. For $-D/2 < Y < 0$, θ vs. Z curve looks like the antisoliton (see Figure 4 of Reference 2). These are summarized in Figure 3(b).

By Eq. (2.10) the velocity profile is given by

$$V_x = \left(\tfrac{1}{2}QY^2 - \frac{\phi_1}{|\gamma_2|}\int\frac{\partial\theta}{\partial T}\,dY\right)\frac{2|\gamma_2|}{\phi_2} + E(X,T) \qquad (5.5)$$

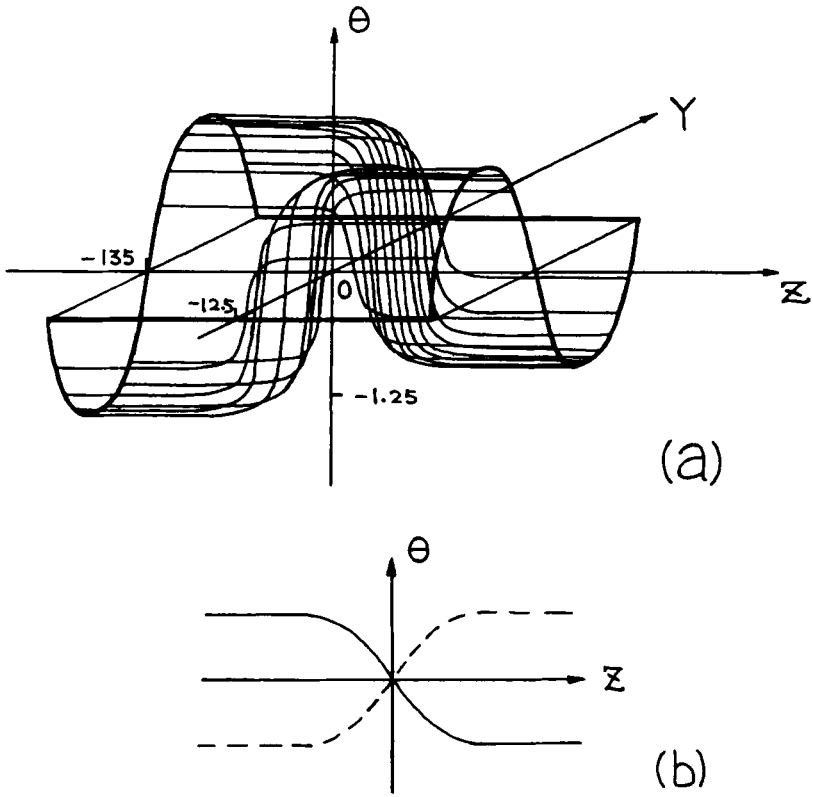

FIGURE 3 (a) Numerical soliton solution of Eq. (5.1). $D = 25$, $Q = 0.03$, $C = 30$. (b) Sketch of θ vs. Z for fixed Y ($Q > 0$, $C > 0$). Solid line: $0 < Y < D/2$. Broken line: $-D/2 < Y < 0$. $\theta = 0$ for $Y = 0, \pm D/2$.

where $V_x \equiv v_x\tau/\lambda$ and E is determined by the boundary conditions of $V_x = 0$ at $Y = \pm D/2$. For a traveling wave $\theta(Z,Y)$, Eq. (5.5) becomes

$$V_x = \left(\tfrac{1}{2}QY^2 + \frac{\phi 1}{|\gamma_2|}\int \frac{\partial\theta}{\partial Z}\,dY\right)\frac{2|\gamma_2|}{\phi_2} + E(Z) \tag{5.6}$$

Note that by Eqs. (2.12) and (2.15), $\phi_1(\theta) = -1/2|\gamma_2|(\gamma + \cos 2\theta) < 0$. $\phi_2 > 0$ for MBBA. For $Q < 0$ and $C > 0$, the velocity profiles of V_x along the x axis are sketched in Figure 4. At $Z = \pm\infty$, the profiles are identical parabols and equal to that of the steady state. At $Z = 0$ where $|\partial\theta/\partial Z|$ (for each Y) is maximum, V_x at $Y = 0$ assumes the largest value. For $Q > 0$ and $C > 0$, the velocities are reversed in direction. When Z is replaced by X in Figures 3 and 4 the configurations shown may be viewed as the patterns at $T = 0$ which then propagate without distortion in the positive x direction with velocity C.

Equation (5.6) and Figure 4 are approximate results. In any case, since near the center of the soliton, $\partial V_x/\partial X$ is non-zero and varies with X Eq. (2.8) implies that there is always a non-zero $V_y = V_y(Z,Y)$ there.

Note that Eq. (2.10) implies that for given $\partial p/\partial x$, under $y \to -y$ one has $\theta \to -\theta$ and $v_x \to v_x$ (in agreement with our Figures 3 and 4). Therefore, no backflows[14] (with $v_x \to -v_x$ when $y \to -y$) are possible. Solutions of Eq. (5.1) other than the type shown in Figure 3 are possible (see Appendix A).

For monochromatic light transmitted through crossed polarizers (with polarization direction at 45° to the x axis) sandwiching the liquid crystal cell, the transmitted light intensity is given by

$$I = I_0 \sin^2(\pi\delta/\lambda_0) \tag{5.7}$$

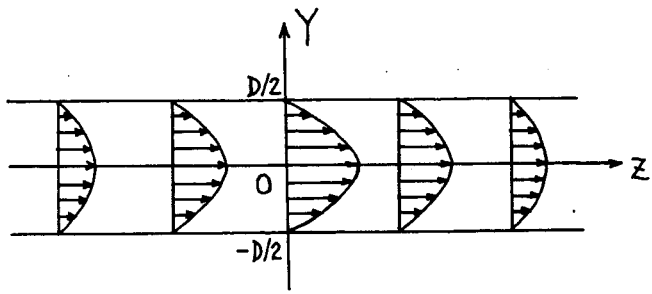

FIGURE 4 Velocity profiles of V_x. $Q < 0$ and $C > 0$.

where λ_0 is wavelength of incident light in vacuum and

$$\delta = \int_{-d/2}^{d/2} dy n_0 \{[1 - (1 - n_0^2/n_e^2) \sin 2\theta]^{-1/2} - 1\} \qquad (5.8)$$

with $n_0(n_e)$ being the index of refraction of the ordinay (extraordinary) light.

The curve I/I_0 vs. Z consists of a series of maxima and minima with unity and zero in magnitude respectively (see Figure 6 of Reference 6). The positions of the points with $I/I_0 = 0.5$ with the region between two adjacent points with a minimum in between painted black are depicted in Figure 5. (These graphs correspond to the black-and-white photographs taken experimentally.) Here, solutions of Eqs. (5.1)-(5.3) similar to that in Figure 3 (with parameters same as in Figure 1) are used in Eq. (5.8) and $n_0 = 1.535$, $n_e = 1.745$ for[15] MBBA are adopted. $\lambda_0 = 6326$ Å. The other parameters are: (a) $d = 22$ μm, $Q = 0.03$, $C = 30$, (b) $d = 36$ μm, $Q = 0.03$, $C = 30$, (c) $d = 36$ μm, $Q = 0.01$, $C = 30$.

For white light, ratio of the transmitted to incident intensities is given by $\int I(\lambda_0)d\lambda_0 / \int I_0(\lambda_0)d\lambda_0$. Without knowing the spectrum of the incident white light, for simplicity, $I_0(\lambda_0)$ is assumed to be independent of λ_0. I/I_0 of several transmitted monochromatic lights are calculated and averaged. Figure 6 shows the results with the parameters of d, Q and C in (a)-(c) the same as that is Figure 5. In the averaging process, seven λ_0's are used. They are $\lambda_0 = 4000$ Å, 4500 Å, 5000 Å, 5500 Å, 6000 Å, 6500 Å and 7000 Å. n_0 is assumed to be independent of λ_0 (see Reference 16) such that $n_0 = 1.535$; n_e as a function of λ_0 is taken from Reference 16. As seen from Figure 6, for the same Q and C, the half-width of the central valley (the dark line) is

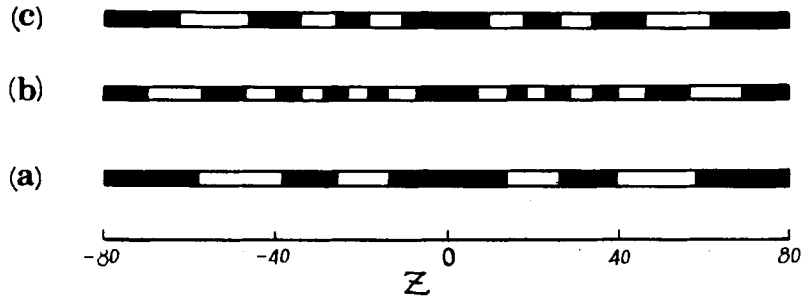

FIGURE 5 Theoretical "photographs" of transmitted monochromatic lights corresponding to single solitons.

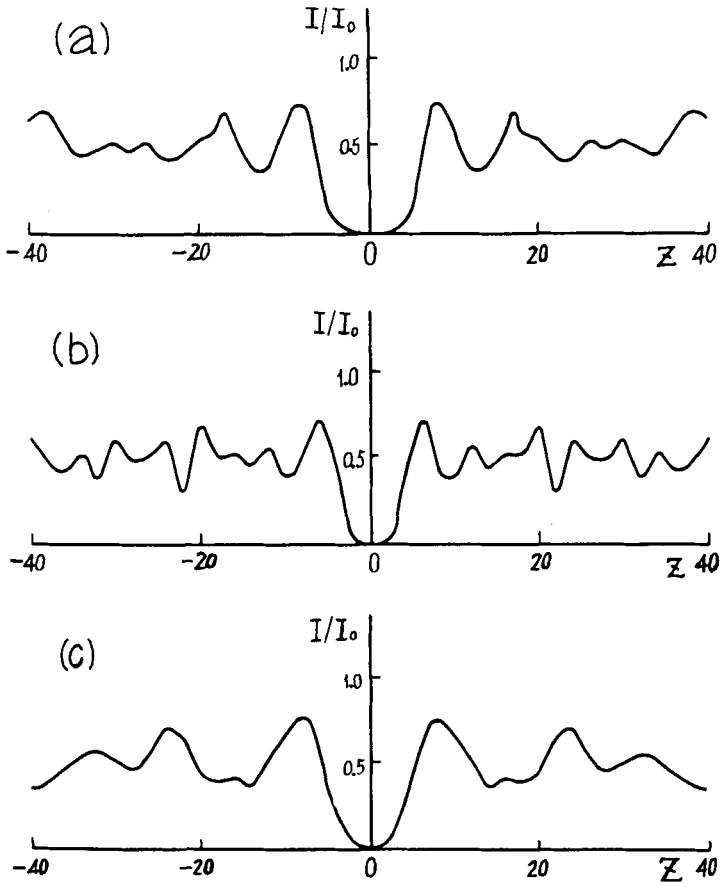

FIGURE 6 Calculated transmitted white-light intensities corresponding to single solitons. Parameters for (a)-(c) the same as those in Figure 5 (see text).

narrower for the thin cell; for the same d and C, the half-width is narrower for larger Q. The $I = 0$ point corresponds to vertical molecules ($\theta = 0$ for all y, the soliton center in Figure 3) which appear as zero in *all* the $I(\lambda_0)$ component curves. While the monochromatic intensity curves may give more information in the distribution of the directors it is the location of the dark line in the white light curve that tells us precisely where the molecules are vertically oriented.

B. Collision of solitons

Solutions of Eq. (2.14) containing two solitons in relative motion are not traveling waves. To describe such a process, we solved Eq. (2.14)

numerically with an initial $\theta(X,Y)$ at $T = 0$ given in Figure 7. The details are presented in Appendix B.

For $Q = 0.03$, the development of the initial data according to the difference equation (B1) shows that the two parts near $\theta = 0$ more or less maintain their shapes but move towards each other (along the x axis) when they are far from each other. As they approach and near each other, the middle part between them flattens out and $\theta(X,Y,T)$ approaches $\theta_s(Y)$, the steady-state solution of Section IV. For fixed Y, the θ vs. X curve transforms with time in a way similar to the annihilation of a pair of $\overline{A}$ solitons in the one-dimensional case.[2] This process is sketched in Figure 8 for $Y > 0$. For $Y < 0$, $\theta \rightarrow -\theta$.

Corresponding to Figures 7 and 8, there will be two dark lines observed with transmitted white light. These two dark lines approach each other and vanish when they meet, as sketched in Figure 9.

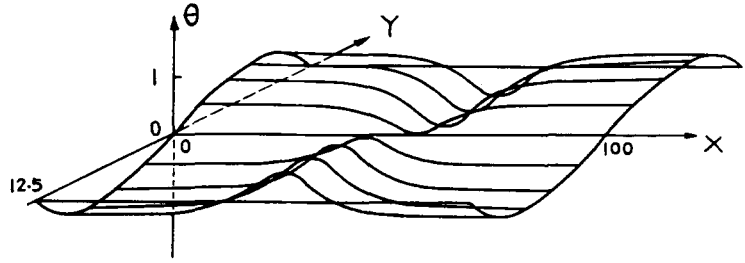

FIGURE 7 Initial state used in the numerical calculation of two colliding solitons.

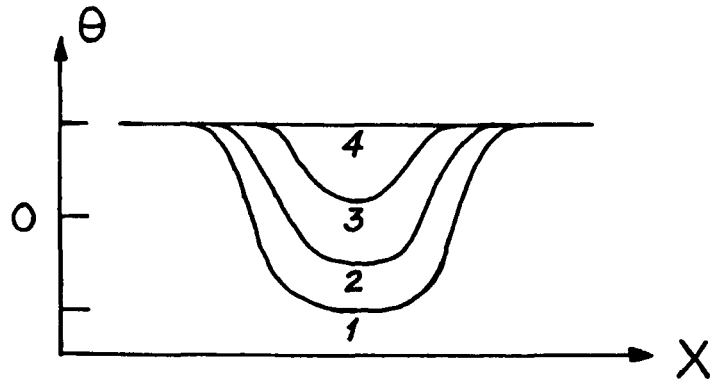

FIGURE 8 Time development of cross-sectional curve θ vs. X for fixed Y. $Y > 0$ and $Q > 0$. As time T increases the θ vs. X curve goes through stages 1, 2, 3 and 4.

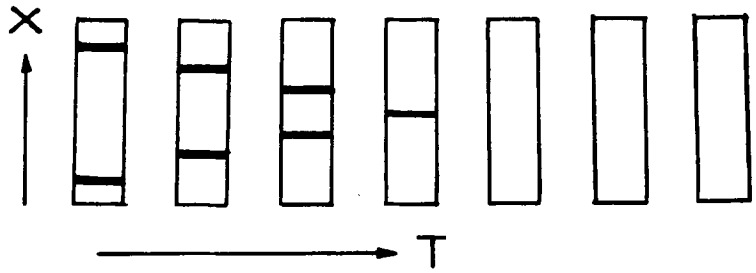

FIGURE 9 Sketch of "photographs" of transmitted white light corresponding to the colliding solitons depicted in Figures 7 and 8.

VI. COMPARISON WITH EXPERIMENTS

In the experiment of Shu, Zhu and Lin,[11] homeotropic MBBA at 25°C in a cell with glass plates of the size 20 cm × 5 cm × 0.5 cm each was used. The cell is sandwiched between crossed polarizers as described in Section V. The separation of the two plates is 22 μm (or 36 μm). Two small holes separated by 14 cm (or 16 cm) are made in the upper plate. Pressures p_1 and p_2 at these two holes located at x_1 and x_2 respectively can be controlled independently or simultaneously. Photographs of transmitted monochromatic or white lights are taken.

For definiteness, let us assume $x_1 < x_2$. In the experiments, p_1 and p_2 are kept at constant values in four different time intervals. Let $p_1 \equiv \bar{p}_0 + a_i$, $p_2 \equiv \bar{p}_0 + b_i$, $i = 1,2,3,4$, where $\bar{p}_0$ is the atmospheric pressure, a_i and b_i are constants within the time interval (t_{i-1}, t_i). $t_0 = 0 = a_1 = b_1$.

In one type of the experiments performed,[11] $b_i = 0$, $a_2 < 0$, $a_3 > 0$, $a_4 < 0$. For example, $a_2 = -6$ cm Hg, $a_3 = 6$ cm Hg, $a_4 = -5.8$ cm Hg. Under white light, in the first stage $[t \in (t_0, t_1)]$, a uniform dark background was observed. In the second stage, a white background was gradually established. Then, in the beginning of the third stage, a dark line was seen running from x_1 to x_2 with its velocity (width) decreasing (increasing) at first but rapidlly approaching a constant. The same phenomena were observed in the fourth stage.

According to our theory in previous Sections, the above observations can be understood as follows. Since $\partial p/\partial x = (p_2 - p_1)/(x_2 - x_1) = (b_i - a_i)/(x_2 - x_1)$, in stage one, $Q = Q_1 = 0$. It is a static situation with all the molecules being vertical. In stage two, a constant pressure gradient of $\partial p/\partial x = -a_2/(x_2 - x_1) > 0$ $(Q = Q_2 > 0)$ is established. An x-independent steady state of the form shown in

Figure 1 is formed eventually. In stage three, one has $\partial p/\partial x = -a_3/(x_2 - x_1) < 0$ ($Q = Q_3 = -Q_2 < 0$) instead. An initial state width $\theta(y)$ given by Figure 1 for $x > x_0$ and $\theta(y)$ given by the reverse of Figure 1 (i.e. $\theta \to -\theta$) for $x < x_0$, where $x_1 < x_0 < x_2$ and x_0 close to x_1, is formed in the beginning. Such a state has $\theta(x)$, for fixed y with $y \in (-d/2, 0)$ and $(0, d/2)$, being a step function and showsup as a very thin dark line under white light. As time increases, such an initial state will travel in the positive x direction according to Eq. (2.14) with $Q = -Q_2$. The step function is now distorted and expanded. The function $\theta(x,y,t)$ eventually evolves into the soliton solution of our Section V in the reversed form of our Figure 3 (i.e. $\theta \to -\theta$). In the process, the width of the cross-sectional curve $\theta(x)$ (for fixed y) near $\theta = 0$ expands with time resulting in an increasing width of the dark line under white light as observed experimentally. When the dark line reaches x_2 before the end of the stage three, an x-uniform state $\theta(y)$ given by the reverse of Figure 1 (i.e. that part of the initial state for $x < x_0$) will occupy the whole cell. In stage four, $\partial p/\partial x = -a_4/(x_2 - x_1) > 0$ ($Q = Q_4 \simeq -Q_3 > 0$) and the whole process of stage three is repeated but with θ replaced by $-\theta$. The fact that $Q_4 \neq |Q_3|$ results in an intial state with the maximum θ's in the two parts of $x < x_0$ and $x > x_0$ slightly differing from each other. The rest is the same. Orientations of the molecules in the cell corresponding to these four stages are sketched in Figure 10.

A typical set of experimental data give $d = 36$ μm, velocity of dark line (under white light) $c = 10$ cm s^{-1}, width of dark line $\delta_{exp} = 0.17$ cm, $|a_i| = 10$ cm Hg, $x_2 - x_1 = 14$ cm. In order to use the numerical solutions obtained in Section V directly, we set $p_0 = 48.2$ dyn cm^{-2}. We then obtain $\lambda = 1.44 \times 10^{-4}$ cm, $\tau = 2.59 \times 10^{-2}$ s and $C\ (\equiv c\tau/\lambda) = 1.8 \times 10^2$, $|Q| \simeq 0.03$ and $D = 25$. The theoretical dark-line width is found to be $\delta_{th} = 0.06$ cm, which is of the same order magnitude as δ_{exp}.

In another type of experiments performed,[11] $a_2 = -b_2 = 7.0$ cm Hg, $a_3 = -b_3 = -6.8$ cm Hg, $a_4 = -b_4 = 6.6$ cm Hg. Phenomena at stages one and two are the same as above. But in the transition form stage two to three, under white light, instead of one single dark line, two dark lines are generated which subsequently travel in opposite direction towards each other. When they meet they merge into one and then vanish altogether. In stage four, same phenomena is repeated.

We have, in this experiment, $Q_1 = 0$, $Q_2 < 0$, $Q_3 > 0$ and $Q_4 < 0$. Stages one and two can be explained as above. In the transition from stage two to three, both a_i and b_i are reversed in sign (in

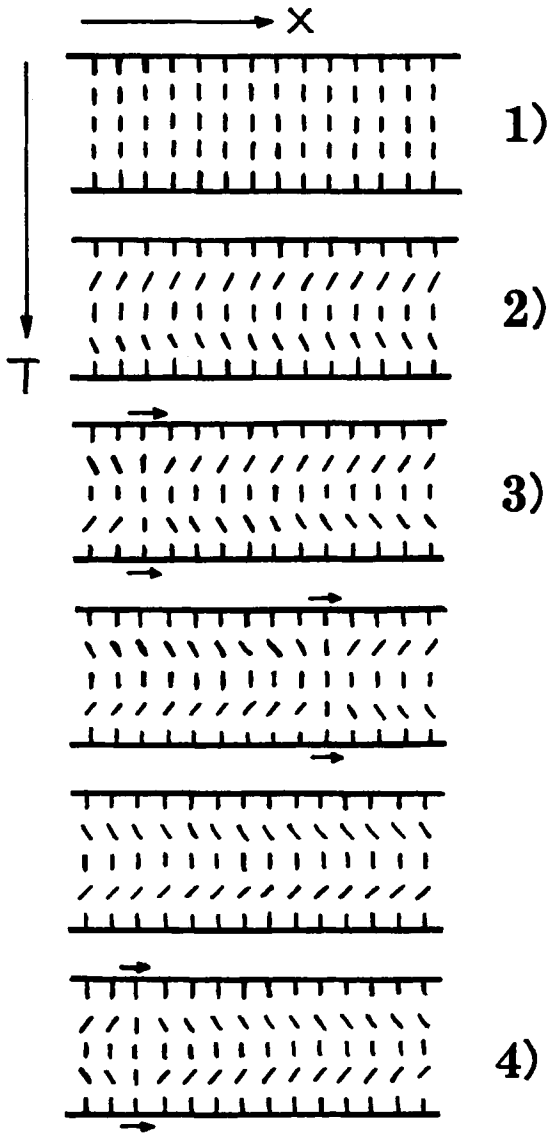

FIGURE 10 Sketch of molecular orientations during the four stages [denoted by 1) to 4)] in the experiments[11] generating a single soliton.

contrast to the previous case in which $b_i = 0$ all the time). An initial state as depicted in Figure 7 is generated. The time evolution of this state discussed in Section VB and shown in Figure 9 corresponds exactly to what was observed. Stage four can be understood similarly.

Note that one actually needs only one hole in the cell to generate single solitons. The essential point is that a_i (or b_i for that matter) should be reversed in sign. Whenever this happens there should be two solitons generated traveling away from the hole in opposite directions. In the experiments of Reference 11 described above, one of these two solitons is blocked by the end of the cell (near which x_1 or x_2 is located). With two holes present and both a_i and b_i reversed in sign we always obtain two solitons. Asymmetric situations (e.g. two colliding solitons meet off the center) can be created by reversing a_i and b_i at different times, say.

A third type of experiments have been carried out[11] in which $a_i = b_i$ and $a_2 = -a_3 = a_4 < 0$. In this case, in stages three and four, two dark lines (under white light) are generated which then collide with each other but merge into one with constant width. This case corresponds to $Q = Q(x)$ and is more complicated. However, it can still be understood[2] within the picture developed in this paper.

Our Figure 5 for monochromatic lights agrees with experiments[11] qualitatively. For higher Q, θ varies more rapidly with x and hence more dark lines in the transmitted light spectrum.

VII. DISCUSSION

Within the assumptions of $M \simeq 0$, $d\theta/dt \simeq \partial\theta/\partial t$ and identical elastic constants we note that Eqs. (2.9) and (2.10) are exact results of Eqs. (2.3) and (2.4) if θ and v_x are uniform in x. (In this case $v_y = 0$.) The approximations of Eqs. (2.9) and (2.10) thus amounts to retaining only two terms related to the x-variations, viz., $K\partial^2\theta/\partial x^2$ and $-\partial p/\partial x$.

In the one-dimensional shearing case,[3,6] the two asymptotic limits of the soliton solution at $x = \pm\infty$ are uniform states of the nonlinear equation of motion (which seems to be also true in other one-dimensional cases[17]). This is no longer true in the two-dimensional case considered here. As shown in Figure 3, while the cross-sectional curve $\theta(Y)$ at $Z \to -\infty$ is of the form expected for the steady-state Eq. (4.1), $\theta(Y)$ at $Z \to \infty$ is definitely not. In this regard, we note that the analytic solution[18] of the two-dimensional sine-Gordon equation shares this property. [Specifically, we mean that the solution given in Eq. (15) of Reference 18 (in which $\sqrt{2}$ should be replaced by $1/\sqrt{2}$) at $\eta \to \pm\infty$ does not satisfy the equation $\partial^2\phi/\partial^2\eta = \sin 2\phi$.]

While the problem considered in this paper is intrinsically two-dimensional in space (because $\partial p/\partial x \neq 0$) the soliton solutions and the physics involved can nevertheless be understood qualitatively by

viewing each layer of the cell (with y fixed) as a one-dimensional system (in x). In other words, the factorization of θ in Eq. (A7) though not exact is a pretty good or useful approximation.

We note that our results do not depend too critically on the specific forms of $f(\theta)$ and $g(\theta)$ in Eq. (2.14) as long as the nonlinear factor $(\gamma + \cos 2\theta)$ in $g(\theta)$ is there. Simplifications may be achieved by replacing $f(\theta)$ and $\phi_2(\theta)$ by constants.

From the results of Section VI, we conclude that our nonlinear equation, Eq. (2.13) or (2.14), is a good description of the experimental data.[11] In particular, solitons are indeed generated and observed by applying pressure gradients in nematics.

Finally, we would like to call attention to the presence of nonlinear waves and solitons in liquid crystals. Their existence has been demonstrated. They will affect the light-scattering spectrum, thermal properties and phase transitons of the systems under consideration, as demonstrated already for other condensed-matter systems.[4,19]

APPENDIX A. NUMERICAL SOLUTIONS OF EQS. (5.1)-(5.3)

Equation (5.1) is replaced by the five-point difference equation,

$$\theta_{i,j} = [2(1 + h^2)]^{-1} \left[h^2\theta_{i+1,j} + h^2\,\theta_{i-1,j} + \left(1 + \frac{1}{2}Ah_z\right)\theta_{i,j+1} + \left(1 - \frac{1}{2}Ah_z\right)\theta_{i,j-1} + BY_i h_z^2\right] \tag{A1}$$

where $h \equiv h_z^2/h_y^2$, h_y and h_z are respectively the separations of the mesh points in the Y and Z directions, $\theta_{i,j} \equiv \theta(Y = Y_i, Z = Z_j)$,

$$A \equiv -C\left[\gamma - \frac{1}{2}(\gamma + \cos\theta_{i,j})^2/\Phi(\theta_{i,j})\right] \tag{A2}$$

$$B = Q(\gamma + \cos 2\theta_{i,j})/\Phi(\theta_{i,j}) \tag{A3}$$

$$\Phi(\theta_{i,j}) \equiv \phi_2(\theta_{i,j})/|\gamma_2| \tag{A4}$$

The boundary conditions Eqs. (5.2) and (5.3) are written in the form of difference equations,

$$\begin{aligned} &\theta_{1,j} = \theta_{m+1,j} = 0, \\ &\theta_{i,1} = \theta_{i,2},\ \theta_{i,n} = \theta_{i,n+1} \end{aligned} \tag{A5}$$

where $D = mh_y$, $2L = nh_z$.

The right-hand side of Eq. (A1) is denoted by

$$H(\theta^l_{i+1,j}, \theta^l_{i-1,j}, \theta^l_{i,i+1}, \theta^l_{i,j-1}, \theta^l_{i,j})$$

which is then taken as

$$\theta^{l+1}_{i,j} = H(\theta^l_{i+1,j}, \theta^l_{i-1,j}, \theta^l_{i,i+1}, \theta^l_{i,j-1}, \theta^l_{i,j}) \tag{A6}$$

Under the conditions of Eq. (A5), Eq. (A6) can be solved iteratively.[20] In Eq. (A6), the superscripts l and $l + 1$ represent the orders of iteration.

To begin the iteration, the initial value is chosen to be

$$\theta^0_{i,j} = \theta_s(Y_i)\, \theta_a(Z_j),\ 1 \leqslant i \leqslant m + 1,\ 1 \leqslant j \leqslant n + 1 \tag{A7}$$

where θ_s is the steady-state solution of Section IV (see Figure 1) and $\theta_a \equiv \bar{\theta}_a/\theta_0$, with $\bar{\theta}_a$ being the A-soliton solution in the case of uniform shearing nematics[3,6] given by

$$\bar{\theta}_a(Z) = \tan^{-1}\{w\tanh[(\gamma - 1)\, wZC]\} \tag{A8}$$

where $w \equiv [(1 + \gamma)/(1 - \gamma)]^{\frac{1}{2}}$ and $C >> 1$. Note that $\theta_a(\infty) = 1$ and $\theta_a(-\infty) = -1$.

The parameters needed in our numerical calculations are chosen according to the material parameters of MBBA and the conditions of the experiments.[11,7] In practice, we have used $D/2 = 12.5$, $L = 135$, $h_y = 0.125$, $h_z = 0.0625$, $Q = 0.0005$-0.03 and $C = 30$-120. The iteration is stopped when the error is less than 0.005 in successive runs.

If in Eqs. (A7) and (A8), $\bar{\theta}_a$ is replaced by the one-dimensional B-soliton solution[6]

$$\bar{\theta}_b(Z) = \cot^{-1}\left\{\frac{1}{w}\tanh\left[-\frac{(1 + \gamma)Z}{wC}\right]\right\} \tag{A9}$$

with $C >> 1$, the C- or D-soliton (see References 2 and 3 for definitions) solution it is possible to obtain traveling wave solutions of Eq. (5.1) other than that shown in Figure 3. For C not satisfying $C >> 1$, the analytic forms of Eqs. (A8) and (A9) are no longer valid, but one can always use the numerical solutions of the one-dimensional A-, B-, C- or D-solitons corresponding to the various possible C values

see Table I of Reference 2 for the domain of C for each type of solitons).

Type A is used here because it is the only one containing vertical molecules and can travel with large velocities (see Section VI).

APPENDIX B. NUMERICAL SOLUTIONS OF TWO COLLIDING SOLITONS

The difference equation corresponding to Eq. (2.14) is

$$\theta_{i,j}^{l+1} = h_1\theta_{i-1,j}^{l} + h_2\theta_{i,j-1}^{l} + h_1\theta_{i+1,j}^{l} + h_2\theta_{i,j+1}^{l} + (1 - 2h_1 - 2h_2)\theta_{i,j}^{l} + (B_1 h_t/A_1)Y_i \tag{B1}$$

where

$$h_1 \equiv h_t(A_1 h_y^2)^{-1},\ h_2 \equiv h_t(A_1 h_x^2)$$

$$A_1 \equiv \gamma - \tfrac{1}{2}(\gamma + \cos 2\theta_{i,j}^{l})^2/\Phi(\theta_{i,j}^{l}) \tag{B2}$$

$$B_1 \equiv Q(\gamma + \cos 2\theta_{i,j}^{l})/\Phi(\theta_{i,j}^{l})$$

Here, h_x, h_y and h_t are, respectively, the separations of mesh points in the X, Y and T directions; Φ is defined in Eq. (A4). Equation (A5) (with h_z replaced by h_x) and the initial condition

$$\theta_{i,j}^{0} \equiv \theta(X_j, Y_i, T = 0) = \phi(X_j, Y_i),$$

$$1 \leqslant i \leqslant m + 1,\ 1 \leqslant j \leqslant n + 1 \tag{B3}$$

are used. ϕ is chosen to be

$$\begin{aligned} \phi(X_j, Y_i) &= \theta_s(Y_i)\,\theta_a(X_j),\ 1 \leqslant j \leqslant n' \\ &= \theta_s(Y_i)\,\theta_{\bar{a}}(X_j),\ n' < j \leqslant n + 1 \end{aligned} \tag{B4}$$

where n' is an integer satisfying $n/2 \leqslant n' \leqslant (n + 1)/2$, θ_s the same as in Appendix A. $\theta_a(X_j)$ is the same as $\theta_a(Z_j)$ but displaced in the X direction. $\theta_{\bar{a}}(X_j)$ is $\theta_a(-X_j)$ and is also displaced in the X direction such that $\theta_a(X_{n'}) = \theta_{\bar{a}}(X_{n'})$. The rapidly varying portions of θ_a and $\theta_{\bar{a}}$ are within the mesh. $A\ \phi\ (X_j, Y_i)$ so chosen is displayed in Figure 7.

In our numerical calculations, $h_t = 0.01$, $h_x = h_y = 0.25$ are used.

References

1. Lin Lei, Invited talk given at Scott Russell Centenary Conference (Solitons '82), Edinburgh, August 22–27, 1982.
2. Lin Lei, Shu Changqing and Xu Gang, Invited talk given at Conference on Transport and Propagation in Nonlinear Systems, Los Alamos, May 21–25, 1984 (to be published in J. Stat. Phys.); and references therein.
3. Lin Lei et al., *Phys. Rev. Lett.* **49**, 1335 (1982); **52**, 2190 (E) (1984).
4. Lin Lei, in Proceedings of the Conference on Statistical Physics and Condensed Matter Theory, Wuhan, China, December 8–14, 1981 (Huazhong Inst. Tech. Press, Wuhan, 1982).
5. Zhu Guozhen, *Phys. Rev. Lett.* **49**, 1332 (1982).
6. Lin Lei and Shu Changqing, *Acta Physica Sinica* **33**, 165 (1984) [English translation to appear in Chinese Phys. (USA)].
7. Shu Changqing, Ph.D. Thesis, Institute of Physics, Chinese Academy of Sciences, Beijing 1984).
8. Shu Changqing, Xu Gang and Lin Lei, *Acta Physica Sinica* (in press).
9. Xu Gang, M.Sc. Thesis, Institute of Physics, Chinese Academy of Sciences, Beijing 1984); Xu Gang, Shu Changqing and Lin Lei, to be published.
10. Xu Gang, Shu Changqing and Lin Lei, *J. Math Phys.* (in press).
11. Shu Changqing, Zhu Guozhen and Lin Lei, to be published.
12. J. L. Ericksen, *Trans. Soc. Rheol.* **5**, 23 (1961); F. M. Leslie, *Arch. Ration. Mech. Anal.* **28**, 265 (1968).
13. L. Lam (Lin Lei), *Z. Physik* **B27**, 349 (1977).
14. F. Brochard, E. Guyon and P. Pieranski, *Phys. Rev. Lett.* **28**, 1681 (1972).
15. Y. Takahashi, T. Uchida and M. Wada, *Mol. Cryst. Liq. Cryst.* **66**, 171 (1981).
16. R. Chang, *Mol. Cryst. Liq. Cryst.* **30**, 155 (1975); He Xuehua, *Wuli* **2**, 107 (1981).
17. P. C. Fife, Mathematical Aspects of Reacting and Diffusing Systems (Springer-Verlag, Berlin, 1979).
18. S. I. Ben-Abraham, *Phys. Lett.* **55A**, 383 (1976).
19. See, e.g., A. R. Bishop, J. A. Krumhansl and S. E. Trullinger, *Physica* **1D**, 1 (1980).
20. G. E. Forsythe, W. R. Wasow, Finite-Difference Methods for Partial Differential Equations (John-Wiley, New York, 1960).